Open Access

Journal of Energy and Power Technology

Research Article

Formation Testing Permeability and Pore Pressure Prediction in Open Hole and Isolated Straddle Packer Applications

Wilson C. Chin *

Massachusetts Institute of Technology, M.I.T., Cambridge, MA, USA; E-Mail: stratamagnetic.software@outlook.com

* **Correspondence:** Wilson C. Chin; E-Mail: stratamagnetic.software@outlook.com

Academic Editor: Grigorios L. Kyriakopoulos

Journal of Energy and Power Technology
2026, volume 8, issue 3
doi:10.21926/jept.2603017

Received: June 20, 2026
Accepted: September 07, 2026
Published: September 11, 2026

Abstract

Knowledge of permeability, which measures a rock formation's resistance to fluid flow, is essential to energy exploration, oilfield development and economic viability, since its value directly relates to cash flow and outlay: the greater permeability is, the faster monetary gains are realized, the lower the initial investment required. Formation testing is crucial to this understanding. It assists with reservoir characterization as it enables direct fluid sampling, reducing the need for resistivity, acoustic and nuclear data, and also because pressure changes measured during pumping can be analyzed with Darcy flow models to predict permeability and pore pressure. The author invented Halliburton's real-time 1997 GeoTap™ model in U.S. Patent 5,703,286 for an *isotropic* permeability "k," one which assumes uniform initial pressure conditions. However, real world environments include overbalanced boreholes whose "supercharged, invading" flows strongly affect events at the *anisotropic* sandface. In practice, dual packers are used to improve predictions by isolating local zones from nearby high pressure surroundings, thus reducing contamination and enabling deeper transient analysis. Within these zones, pressures are high but *constant*, providing a key entry point for math modeling. This paper extends the 1997 model, so that a newer exact, closed form, analytical "forward" method is available to predict pressure fields when formation parameters are inputted, *and* which improves "inverse models" to help predict permeability and pore pressure under highly supercharged conditions when (pressure, time) pairs are known at the source probe, also demonstrating how synthetic data from forward analysis can be used to validate overall workflow and inverse development strategies. How the new *approximate* models relate to recent, more complete 2024 azimuthal multiprobe models requiring substantial computation is also explained, with the aim of facilitating drilling and well logging operations and more effective reservoir characterization. The present work provides a rapid and convenient platform for field use, just as the 1997 GeoTap™ model simplified both math and physics for use during initial logging when fewer input modeling parameters are available. We additionally review our recent 2024 azimuthal multiprobe methods which fully account for dynamic invasion, transient mudcake growth and multiphase effects, which again complement the approximate tools developed here to estimate permeability. Quantifying these effects with the approximate model allows oil companies to rapidly formulate drilling and production programs, leaving more complete analysis to detailed models only when satisfactory input data are available. The combined tools support cost effective processes in commercializing newly discovered resources, thus improving on an understanding essential to energy exploration, oilfield development and economic productivity.

Keywords

Dual packer; formation testing; LWD; MWD; permeability prediction; pore pressure; pressure transient analysis; straddle packer

1. Introduction, Background and Modeling Challenges

Drilling and exploration in oil and gas are important to societal progress, economic and infrastructure development. An understanding of the reservoir and how petroleum fluids flow as a function of viscosity and permeability is critical. This most relevant flow property, recognized early on by industry leaders, has motivated continual improvements in well logging. Until the mid-1990s, permeability estimates were obtained from pressure drops and flow rates measured from rapid steady flow field tests. However, as newly discovered resources presented heightened resistance to flow, such tests consumed increasing time and logging expense. In 1997, this author introduced real-time permeability prediction through Halliburton's U.S. Patent 5,703,286, supporting a commercially successful GeoTap™ service. This provided rapid, convenient and accurate permeability and pore pressure estimates, allowing operators to log wells with higher point densities and efficiency while reducing the need for resistivity, acoustic and nuclear measurements. However, the method does not apply to overbalanced wells, and this limitation has hindered energy exploration and oilfield development for three decades. But much more is affected-when energy costs increase, society is negatively impacted.

Figure 1(left) describes many conventional drilling processes. A formation tester nozzle is pressed against the formation and removes reservoir fluid. The borehole wall is cased or otherwise impenetrable. Pressure transients recorded during withdrawal are analyzed with Darcy models to predict permeability, pore pressure, porosity and compressibility. Three-dimensional CFD solvers, requiring tedious geometric setup, repeated simulations, and computer resources, are nonetheless mesh dependent – change the grid, the answer changes. Moreover, round-off and truncation errors contribute to “artificial viscosity,” so-called by 1940s computer pioneer John von Neumann, which affect computed pressure fields and properties prediction. The alternatives are simplified math models, offering unique, rapid, stable and easy to use solution in the spirit of GeoTap™. Figure 1(right) displays the spherical flow model used for isotropic media by generations of petrophysicists. Required changes are described next.

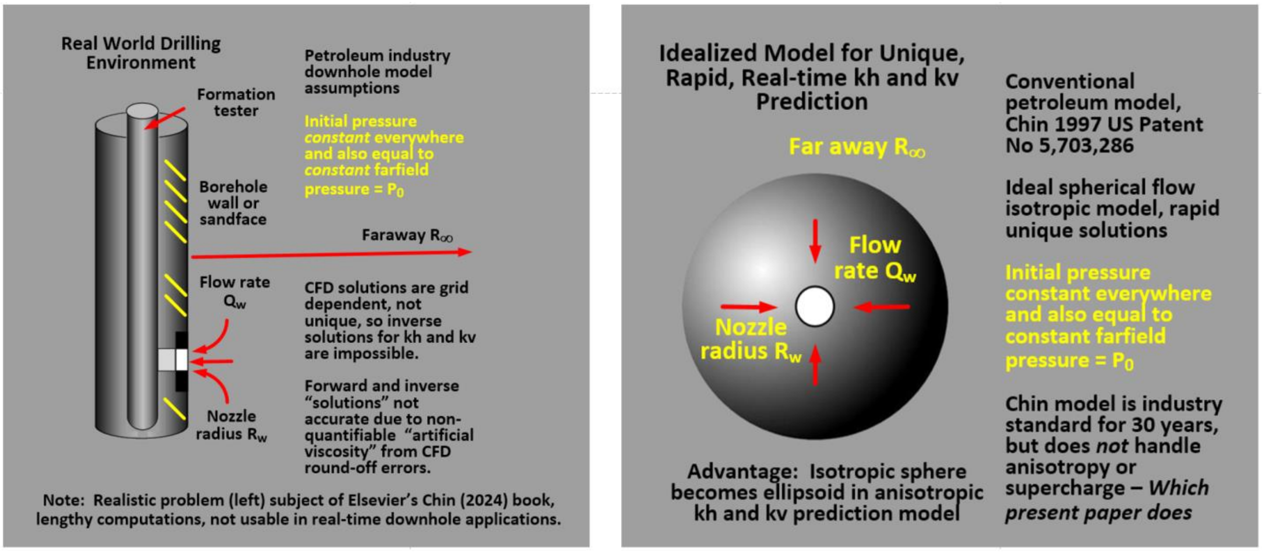

Figure 1 Actual drilling scenario versus simplified model.

In GeoTap™ the governing partial differential equation $p_{rr} + 2/r\ p_r = \phi\mu c p_t$ depends only on a single “r” radial coordinate and time “t”. This invariably leads to simple algebraic solutions. The nozzle, whatever its geometry, circular, oval or slotted, is represented by a small centered source of radius R_w which, importantly, is what Nature “sees” at a distance. The auxiliary conditions are simple: a constant P_0 pore pressure in the far-field, equal to a similarly constant initial pressure, in addition to a volume flow rate specification Q_0 prescribed at R_w. Aside from Muskat [1]’s seminal contributions early on, other well-known papers on spherical flow modeling are available, e.g., Dake [2], Scheidegger [3], Streeter [4] and Yih [5]. In 1997, this author introduced a real-time *isotropic* method in Halliburton’s U.S. Patent 5,703,286 (see Proett, Chin and Chen [6]), supporting the company’s commercially successful GeoTap™ service. Extensions for transversely isotropic media with flowline storage and surface skin effects appeared in Proett, Chin and Mandal [7] but a solution strategy was not available at the time. Experimental validations were only given later in Lee [8]. These two works were differential equation models instead of the heuristic statements used by engineers.

However, these formulations would require refinement. Not long after, Rourke et al. [9], in detailed field studies undertaken in the Gulf of Thailand, would find hundreds of wells with “overbalance” pressures in the 2,000 psi range (the terms overbalance, invasion and supercharge are often used interchangeably) In addition, wells can also be “underbalanced.” These possibilities required a more general formulation, as suggested in Figure 2(left). There, overbalance arises from rapid vertical pressure changes due to high density muds used to restrict formation fluid outflux. Figure 2(right) describes the use of “packers,” essential to completions, safety and well integrity. Aside from flow isolation, the arrangement allows pressures to equalize in the yellow interval so that a single constant pressure applies. We take advantage of this simplifying result in our math modeling.

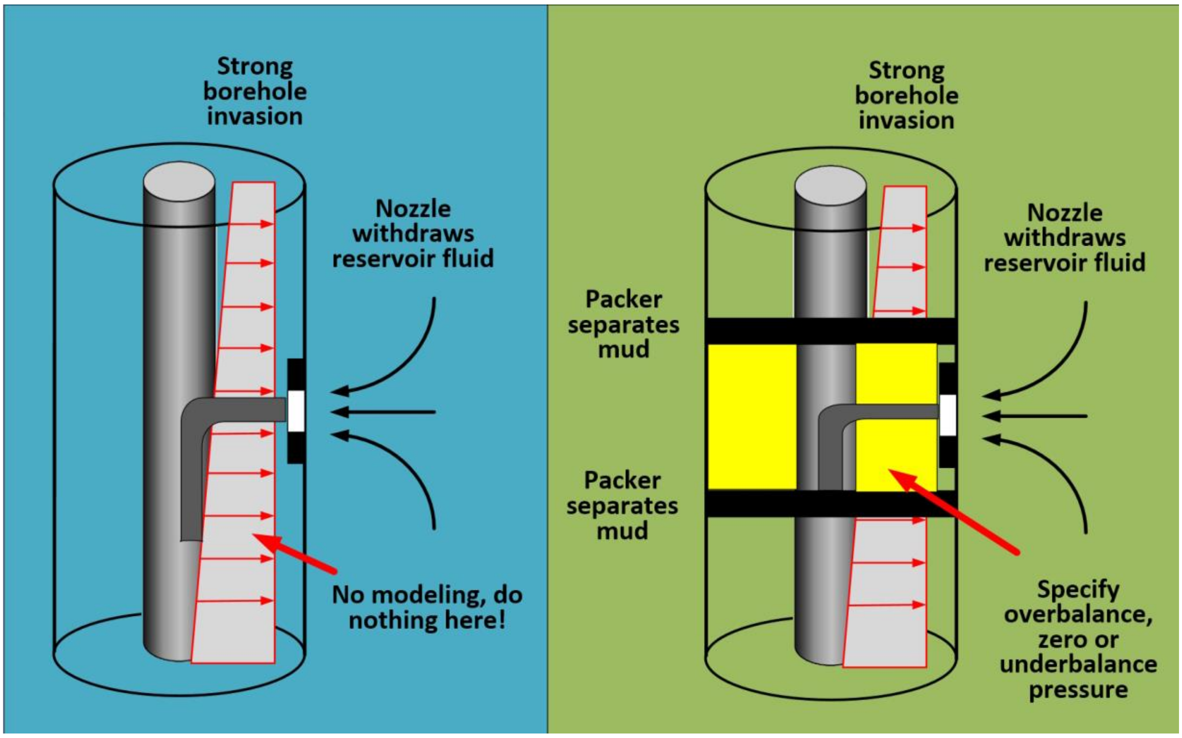

Figure 2 Formation tester nozzle in open hole versus isolated space between packers.

When significant overbalance is present, permeability prediction methods like GeoTap™, which assume constant initial pressures, no longer apply. Such methods give inaccurate permeabilities and incorrect pore pressures as shown in five later calculations. Two challenges arise. As for Figure 1, detailed geometric resolution will require CFD approaches, which again are not useful because of mesh dependencies. The second challenge is a need for simplicity, solution uniqueness hosted by analytical formulations, and rapid, stable calculations useful in field operations. In short, is it possible to design a model that reduces to Figure 1(right) in the limit of zero overbalance? It is clear that compromises will be required, but such are tolerable so long as correct physical trends can be predicted and comparative numbers for permeability and pore pressure are available to guide drilling and formation evaluation objectives.

We now turn to the isotropic formulation of Proett, Chin and Chen [6], for which an "exact," closed form analytical solution in terms of "complex complementary error functions" was offered. (By "exact," we refer to the closed form, analytical nature of the 1997 solution rather than full adherence to the actual downhole physics.) We described this problem earlier, and the 1997 reference states this, as follows,

$$\partial^2 P(r,t)/\partial r^2 + 2/r \partial P/\partial r = (\phi \mu c/k) \partial P/\partial t \tag{1}$$

$$P(r, t=0) = P_0, r > R_w \tag{2}$$

$$P(r=\infty, t) = P_0 \tag{3}$$

$$(4\pi {R_w}^2 k/\mu) \partial P(R_{w,} t)/\partial r - VC \partial p/\partial t = Q_0 \tag{4}$$

Again, P is pressure, r is spherical radius, t is time; ϕ, μ, c and k are porosity, viscosity, compressibility and isotropic permeability; R_w is "spherical well" radius, V is flowline volume, C is flowline fluid compressibility, Q_0 is a constant volume flowrate. Equation 1 describes mass conservation, Equation 2 assumes constant pressure initial conditions, Equation 3 imposes a uniform farfield pore pressure, while Equation 4 modifies "$(4\pi R^2k/\mu)\partial P(R_W,t)/\partial r = Q(t)$" (or simply "Area × Velocity = Flow Rate") with "$VC\, \partial P/\partial t$" to model flowline fluid compression and expansion. Only Equation 2 requires modification: but why, and under what restrictions?

In our method, we replaced $P(r,t = 0) = P_0$, $r > R_W$ with a *simple* slightly modified $P(r,t = 0) = P_0 + Z/r$, where $Z = (P_{bh} - P_0)R_W$. Here, P_{bh} represents borehole pressure, which can be greater (overbalance) or less than (underbalance) P_0. If $P_{bh} = P_0$, then Z vanishes and Equation 2 is recovered. *Why is this justifiable?* Imagine a situation where, as in Figure 1(left), the borehole sandface is completely cased or a thickened mudcake has sealed the formation from further invasion. Then, only the isolated yellow region between packers in Figure 2(right) "sees" the exposed formation. Because it still contains (constant) high pressures with $P_{bh} > P_0$, invasion occurs. In the context of Figure 1(right), spherical flow is ongoing. If in this volume, steady-state is reached, Equation 1 becomes $\partial^2P(r,t)/\partial r^2 + 2/r\, \partial P/\partial r = (\phi\mu c/k)\partial P/\partial t \approx 0$, from which we $P(r,t = 0) = P_0 + Z/r$ taken earlier. In summary, this initial condition implicitly assumes a largely sealed wellbore, implying a simplified "$P_0 + Z/r$" function that reduces to P_0 as in the zero overbalance limit of Equations 1-4. Our choice is approximate. In reality, continual slow invasion, nozzle shape effects, and so on, will introduce finite but tolerable uncertainties.

This formulation appeared in Chin [10], where its advantages are noted (pp. 69-77). The "exact," closed form, analytical, zero-overbalance solution in Proett, Chin and Chen [6], discussed in detail in Chin et al. [11], is given later in this paper because *both overbalance and anisotropic solutions can be expressed in terms of its fundamental solutions*. The basic initial-boundary value problem, now comprising of Equations 1, 3, 4 and "$P(r,t = 0) = P_0 + Z/r$," proved formidable analytically. *Ultimately, we transformed this problem into one with constant (and not spatially dependent) initial conditions as in Equation 2, with "Z/r" effects now incorporated into a modified flow rate "$Q(t) + 4\pi kZ/\mu$." Anisotropic modifications required only special coordinate transforms and renormalizations to take isotropic form.* Thus, the 1997 solution reproduced later was used to advantage. From a practical perspective, software changes are reduced, and solutions remain compact, rapid and stable. The required algebra, however, was extremely tedious. Thus, lengthy equation details, including definitions for re-defined normalizations, offered in the 1997, 2014 and 2019 references, will not be duplicated here.

We refer to Equations 1-4 and now indicate the steps used to derive key equation solutions. These were obtained by Laplace transforming Equation 1 in time, solving the resulting second-order differential equation using Bessel functions, inverting the inverse transform, and applying boundary conditions. The explicit solutions are useful because overbalance effects (and also, transversely isotropic extensions, as we show shortly) can be incorporated with straightforward modifications. Continuing, we first rewrote Equations 1-4 in dimensionless form, that is,

$$\partial^2 p(r,t)/\partial r^2 + 2/r\ \partial p/\partial r = \partial p/\partial t \tag{5}$$

$$p(r,0) = 0 \tag{6}$$

$$p(\infty,t) = 0 \tag{7}$$

$$\partial p(r_w,t)/\partial r - \partial p/\partial t = F(t) \quad (8)$$

This is free of explicit parameters except for a dimensionless radius r_w = $4\pi R_w^3\phi c/(VC)$ appearing only in the argument of Equation 8. Following the above steps, we found

$$p_{exact}(r_w,t) = \{1/(\beta_1-\beta_2)\}\{\beta_1{}^{-1} - \beta_1{}^{-1}\exp(\beta_1{}^2 t)\operatorname{erfc}(\beta_1\sqrt{t}) \\ -\beta_2{}^{-1} + \beta_2{}^{-1}\exp(\beta_2{}^2 t)\operatorname{erfc}(\beta_2\sqrt{t})\} \quad (9)$$

$$p_{exact}(r,t) = \{r_w/(r(\beta_1-\beta_2))\} \\ \times \{\{-\exp\left(\beta_1{}^2 t - \beta_1(r-r_w)\right)\operatorname{erfc}(\beta_1\sqrt{t} + (r-r_w)/(2\sqrt{t})) + \operatorname{erfc}((r-r_w)/(2\sqrt{t}))\}/\beta_1 \\ -\{\exp\left(\beta_2{}^2 t - \beta_2(r-r_w)\right)\operatorname{erfc}(\beta_2\sqrt{t} + (r-r_w)/(2\sqrt{t})) + \operatorname{erfc}((r-r_w)/(2\sqrt{t}))\}/\beta_2\} \quad (10)$$

Here $\beta_1 = +1/2 - 1/2\sqrt{1-4r_w^{-1}}$ and $\beta_2 = +1/2 + 1/2\sqrt{1-4r_w^{-1}}$ are *complex* constants. The "erfc" refers to "complex complementary error functions" with complex arguments. Equations 9 and 10 express pressure in terms of permeability, useful in "forward" problems where pressures are solved with formation, tool and rate inputs are given. *Having these explicit equations also allows expression of, say permeability as a function of pressure, important when "inverse" calculations are performed with (pressure, time) pairs available at specific locations.* This requires simpler math expansions, obtained from Taylor series and asymptotic methods.

$$p(r_w,t)_{early-time\ from\ exact} = -t + 4t^{3/2}/(3\sqrt{\pi}) + (1-r_w)t^2/(2r_w) \\ +8(r_w-2)t^{5/2}/(15r_w\sqrt{\pi}) + \cdots \quad (11)$$

$$P(R_w,t)_{early-time\ from\ exact} = P_0 - Q_0 t/(VC) \quad (12)$$

$$p(r_w,t)_{late-time\ from\ exact} = -r_w + r_w{}^2/\sqrt{(\pi t)} + (2-r_w)r_w{}^3/(2t^{3/2}\sqrt{\pi}) \\ +3r_w{}^4(r_w-1)(r_w-3)/4t^{5/2}\sqrt{\pi} + \cdots \quad (13)$$

$$P(R_w,t)_{late-time\ from\ exact} = P_0 - Q_0\mu/4\pi R_w k + \{Q_0\mu/(4\pi k)\}\sqrt{\{\phi\mu c/(\pi k t)\}} + \cdots \quad (14)$$

Late-time solutions are independent of flowline storage V and compressibility C, depending only on transport properties like viscosity and permeability. Early-time solutions as in Equation 12 depend only on V, C and Q_0 (this is used for compressibility prediction). Intermediate-time solutions, from which permeability is derived, not shown but presented in Chin et al. [11], do not depend on V, c, C and ϕ. Thus, there are three inverse algorithms, each requiring only its own subset of the inputs used in Equations 9 and 10. Our "inverse simulator" is actually three.

We noted above that supercharge results are modeled from slightly different normalizations, and using the altered "Q(t) + 4πkZ/μ" instead of Q_0. We also noted that Equations 9 and 10 apply to transversely isotropic media, again using slightly different normalizations together with coordinate transformations. We outline the steps needed to accomplish this. A more complicated kh ($\partial^2 P(x,y,z,t)/\partial x^2 + \partial^2 P/\partial y^2$) + kv$\partial^2 P/\partial z^2$ = ϕμc∂P/∂t models "transversely isotropic" media in comparison to Equation 1, where kh and kv are horizontal and vertical permeabilities. Using a polar coordinate mapping from multivariable calculus, this transforms into "$\partial^2 P(r,t)/\partial r^2 + 2/r\ \partial P/\partial r = (\phi\mu c/k)\partial P/\partial t$," taking a simpler isotropic form, where "r" is an ellipsoidal as opposed to spherical radius, and "k" now referring to an "effective" $k_{eff} = kh^{2/3}kv^{1/3}$. For isotropic media, the "$(4\pi R_w^2 k/\mu)\partial P/\partial r$" in Equation 4 now involves more than multiplying the velocity $(k/\mu)\partial P/\partial r$ by the area $4\pi R_w^2$. The "scalar, dot product" between (i) the Darcy velocity q (expressed in terms of spherical ∇P components), and (ii) the unit normal n to the ellipsoidal surface "z = f(x,y)" must be taken at all ellipsoidal surface points and integrated over the enclosed volume. The algebra is tedious, but a dimensionless *p* can be found that satisfies Equations 5-8 although with different dimensionless parameters. This completes the steps needed to derive a closed form solution modeling flowline storage, overbalance pressure, as well as transversely isotropic effects.

2. Experimental Validations, Synthetic Data, Software Modules and Workflows

The above summaries focus on mid-1990s to 2010 work, starting with the Halliburton GeoTap™ patent in Proett, Chin and Chen [6], SPE and SPWLA studies on single-phase flow, ideal source models, then skin effects and multiple flow rates, subjects not reviewed here. These led to three books in Chin et al. [11], Chin [12] and Chin [10]. Our focus was redirected toward azimuthal multiprobe tools in finite diameter boreholes, i.e., effects like supercharge, dynamic mudcake controlled invasion, coupled pressure transient and contamination multiphase models. These led to the books Lu et al. [13], Lu et al. [14] and Chin [15]. This paper bridges these sets of book publications by introducing a simplified transient model incorporating *ideal source* and *strong supercharging* useful to field operations.

Throughout our research, practical issues were motivated by two works. One was Rourke et al. [9], where field studies pointed to the prevalence of overbalance and supercharging in the Gulf of Thailand, showing excess pressures of 2,000 psi identified in numerous wells. The second was Lee [8], a Doctoral Thesis published at The University of Texas at Austin, summarizing experimental laboratory results and applications of formation tester measurements in the presence of mud filtrate invasion. *This work would validate the present author's 1997 formulations, methods and model, providing impetus to additional research along formal differential equation based lines. Both this author's and Lee's work were supported by Halliburton Energy Services, and both engaged in informal contact over a period of years*. While the lab work was important, the efforts were time-consuming and expensive. Experimental validations are not practical on a routine basis, and particularly for high overbalance pressures, where 2,000 psi excess pressures are difficullt to achieve in lab environments. The need for some type of validation, of course, motivated us to draw upon the resources at hand. For one, the author had access to Equations 9 and 10, which represent "exact," closed form, analytical solutions to isotropic formations, at least under spherical source conditions. With Lee's lab based success, we were confident that our exact analytical solutions can, to a great extent, serve as the focal point for validations underlying predictive methods. These error function solutions are "exact," in the same way solutions like $y(t) = A\sin\omega t + B\cos\omega t$ to $y''(t) + \omega^2 y = 0$ are "exact." That both require detailed table (or scientific library evaluation) does not change this fact. Understanding this, together with Lee's validating experiments, we formulated a practical and rapid means to evaluate the quality of our permeability methods.

The final "recipe" is easily summarized. We introduce a "forward solver," that is, one that calculates exact pressures (say, using Equations 9 and 10, or their extensions to anisotropy and overbalance) when input parameters like permeability, pore pressure, porosity, compressibility, plus hardware and rate inputs are given. The forward solver creates "synthetic solutions," which play the role of pressures measured in field work or lab experiments. The exact forward solver depends on *all* inputs like ϕ, μ, k, c, C, V, flow rate Q_0, nozzle radius, pore pressure, initial conditions, and so on. Drawing on our above experience with asymptotic solutions, we understand that *pressures in different time ranges are controlled by different properties*. For instance, Equation 12 states that compressibility can be simply evaluated using "early time" data related to V and Q_0. "Late time" pressures, for example, are independent of V and C, but may involve porosity. "Intermediate time" pressures (used in permeability prediction) do not depend on c, C, V or ϕ. "inverse solvers," which require (pressure, time) data at a point in space, and solve for properties like permeability and pore pressure, are designed using appropriate asymptotic solutions. If our intermediate time solution (which does not require c, C, V or ϕ) correctly predicts permeability and pore pressure, this provides a high degree of credibility indicating correct math and physics. One might argue that the strategy behind our validations is circular, but then, Darcy's Equations 1-4 underpin both forward and inverse approaches, in much the same way that a general "F = ma" underpins forward and inverse mechanical models.

3. Validations and Calculated Results

We present five suites of "*correct supercharge* versus *incorrect conventional* model" comparisons illustrating differences in predicted pore pressure and effective permeability. The examples range from very low to high formation mobilities. Within each suite, a forward simulator first calculates "synthetic pressures," or numbers that would be measured in actual well logging. Three (pressure, time) data pairs are selected along pressure transient curves from which pore pressure and mobility are predicted using our inverse algorithms. We also give detailed numerical studies affirming the consistency between exact analytical *forward* solutions and approximate, rapid and convenient *inverse* solutions for a range of mobilities. In particular, the mobilities 0.001, 0.01, 0.1, 1 and 10 are studied. Exact forward solutions are first calculated numerically. Then, our overbalance, supercharge inverse algorithm is evaluated with the known over-pressure P_{over} correctly specified, in all cases showing permeability and pore pressure recovery are good. That is, imverse parameters predictions are almost identical to the same inputs assumed in the forward code. This occurs with c, C, V or ϕ omitted from inverse inputs, parameters usually unavailable in the field (an inverse solver requiring such parameters will not be usable in practice). In the course of our validations, we observed a useful property offering high potential: *late dimensionless times may overlap with early dimensional physical times.* Since the normalizations in dimensionless times vary with application, this implies that late time formulas normally not used at, say, 10 sec to 1 min, may apply very well. Users should not confuse subjective human judgments with mathematical semantics. A "late time expansion" may well apply to "10 sec," a possibility that is easily evaluated by our forward simulator.

Additionally, we found the following references useful in our mathematical work-Abramowitz and Stegun [16], Bateman [17], Carnahan, Luther and Wilkes [18], Churchill [19], IMSL [20], Pipes [21] and Press et al. [22]. In well testing, the related works were excellent-Goode and Thambynayagam [23], Horne [24], Joseph and Koederitz [25], Kasap [26], Kasap et al. [27], Moran and Finklea [28], Peaceman [29], Proett and Waid [30], Raghavan [31], Sabet [32], Schlumberger

[33], SPWLA [34, 35], Stanislav and Kabir [36] and Streltsova [37]. For convenience, Table 1 describes the meanings of different parameters used in our analysis.

Table 1 Formation Testing Input Parameters.

C	Compressibility (flowline)	P_{bh}	Pressure (borehole)
c	Compressibility (formation)	P_{over}	Pressure (overpressure)
V	Flowline volume	P_0	Pressure (pore)
GF	Geometric factor	R_w	Radius (spherical well)
m	Mobility	x	Spatial x direction
∂	Partial derivative symbol	y	Spatial y direction
k	Permeability	z	Spatial z direction
k_{eff}	Permeability (effective)	r	Spatial r direction
k_h	Permeability (horizontal)	θ	Spatial θ azimuthal
k_v	Permeability (vertical)	t	Time
ϕ	Porosity	μ	Viscosity
P	Pressure	Q	Volume flow rate

3.1 Example 1: Mobility = 0.001 md/cp Calculations (Very, Very, Very Tight Zone)

In Example 1, we first solve our “FT-PTA-FastForward (forward) Simulator” assuming a mobility of 0.001 md/cp in Figure 3. A dynamically insignificant hydrostatic pressure of 100,000 psi is selected in Figure 3 for convenience (so that drawdown pressures remain positive for graph plotting and data entry purposes) in this very tight formation drawdown example. In the computed results for this single source probe problem, we arbitrarily select three moderately separated red “pressure and time” pairs before 30 sec in Figure 4. *Generally, we select data at t = 0, “final t,” and an intermediate time, with differences in predictions less than 2% at most*. Figure 5(upper) shows these inputs in “inverse” code FT-PTA-DD-SC along with other parameters that do *not* include ϕ, c, C and V, as explained earlier in Section 2. We entered the overbalance pressure P_{over} = 2,000 psi in the *upper* inverse menu. The caption in Figure 5 indicates excellent results for predicted mobility and pore pressure. In the *lower* inverse menu, an incorrect “$P_{overbalance}$ = 0” as assumed in conventional models leads to incorrect results.

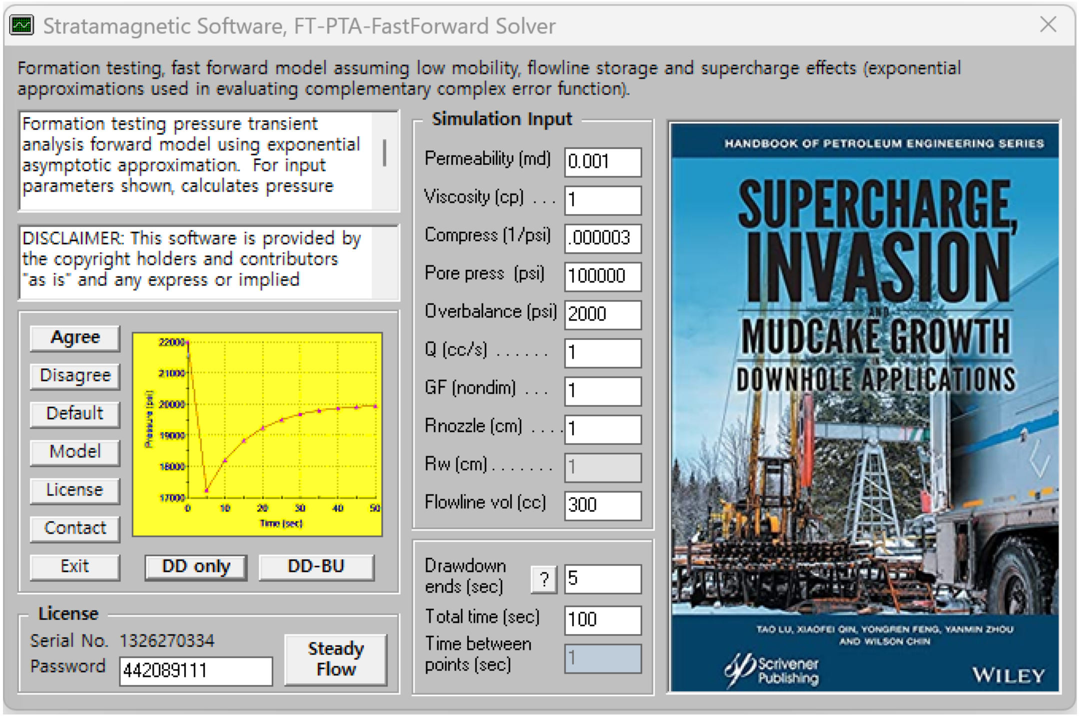

Figure 3 Mobility = 0.001 md/cp input assumptions for forward analysis.

```
Fluid, formation, tool and pumping parameters ...

Formation permeability .......... (md):    0.1000E-02
Viscosity ...................... (cp):    0.1000E+01
Liquid compressibility ....... (1/psi):    0.3000E-05
Pore pressure ................. (psi):    0.1000E+06
Overbalance pressure .......... (psi):    0.2000E+04
Volume flow rate ............. (cc/s):    0.1000E+01
Probe radius ................... (cm):    0.1000E+01
Geometric factor ..... (dimensionless):    0.1000E+01
Effective radius ............... (cm):    0.1000E+01
Flowline volume ................ (cc):    0.3000E+03
Total simulation time ......... (sec):    0.1000E+03
Graph every N sec, where "NSEC" equals:    0.1000E+01
```

T(sec)	P(psi)
0.0	102000.
1.0	100888.
2.0	99776.
3.0	98666.
4.0	97556.
5.0	96448.
6.0	95341.
7.0	94235.
8.0	93130.
9.0	92026.
10.0	90923.
20.0	79950.
30.0	69082.
40.0	58317.
50.0	47654.
60.0	37092.
70.0	26630.
80.0	16268.
90.0	6004.

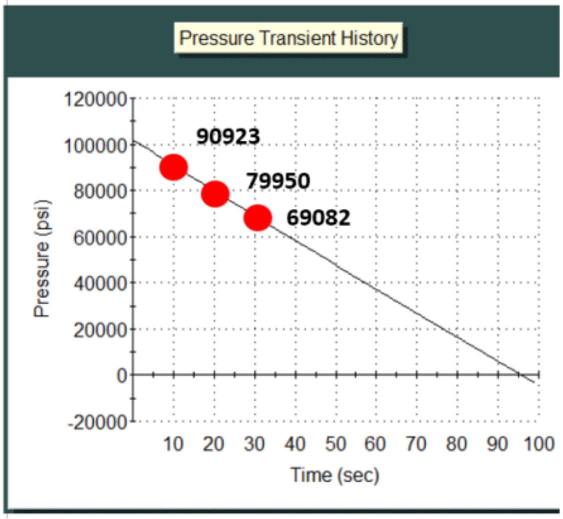

Figure 4 Computed forward pressure response at single pumping probe.

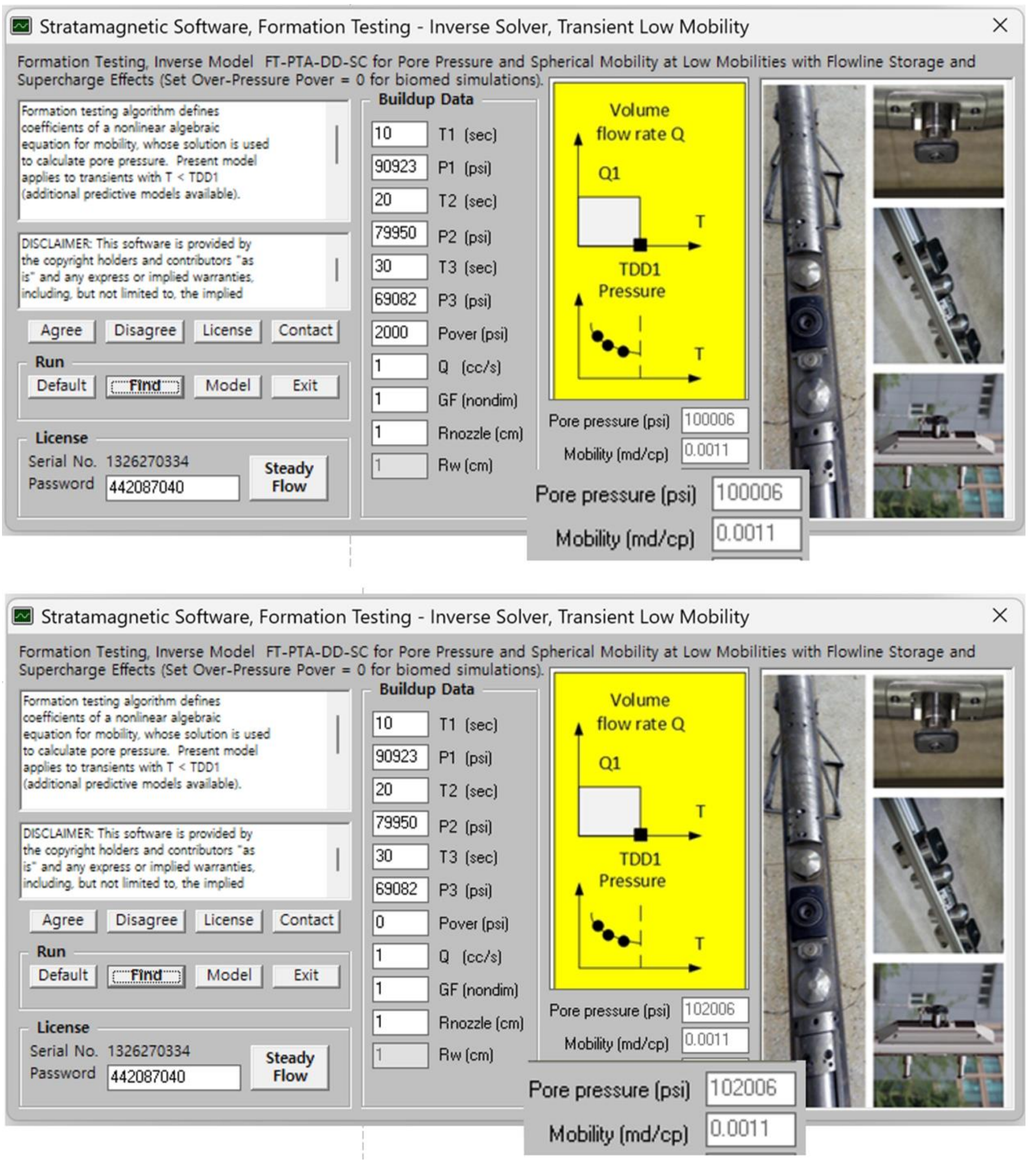

Figure 5 Mobility = 0.001 md/cp calculation. Note ϕ, c, C and V inputs are not required for inverse mode. *Upper*, P_{over} = 2,000 psi is inputted, predictions P_0 = 100,006 psi and mobility = 0.0011 md/cp both correct (inputs were 100,000 and 0.001). *Lower*, assumed P_{over} = 0 psi is incorrect, corresponding to conventional GeoTap™ type simulators. The prediction P_0 = 102,006 psi is incorrect by 2,006 psi, while the predicted mobility = 0.0011 md/cp is correct.

3.2 Example 2: Mobility = 0.01 md/cp Calculations (Very, Very Tight Zone)

In Example 2, we first solve our "FT-PTA-FastForward (forward) Simulator" assuming a mobility of 0.01 md/cp in Figure 6. A dynamically insignificant hydrostatic pressure of 100,000 psi is selected in Figure 6 for convenience so that drawdown pressures remain positive in this very tight formation drawdown example. In the computed results for this single source probe problem, we arbitrarily select three widely separated red "pressure and time" pairs in Figure 7. Figure 8(upper) shows these inputs in "inverse" code FT-PTA-DD-SC along with other parameters that do *not* include ϕ, c, C and V, as explained earlier in Section 2. We entered the overbalance pressure P_{over} = 2,000 psi in the upper inverse menu. The caption in Figure 8 indicates excellent results for predicted mobility and pore pressure. In the lower inverse menu, we entered an incorrect P_{over} = 0 psi corresponding to conventional zero-overbalance models and obtained incorrect results.

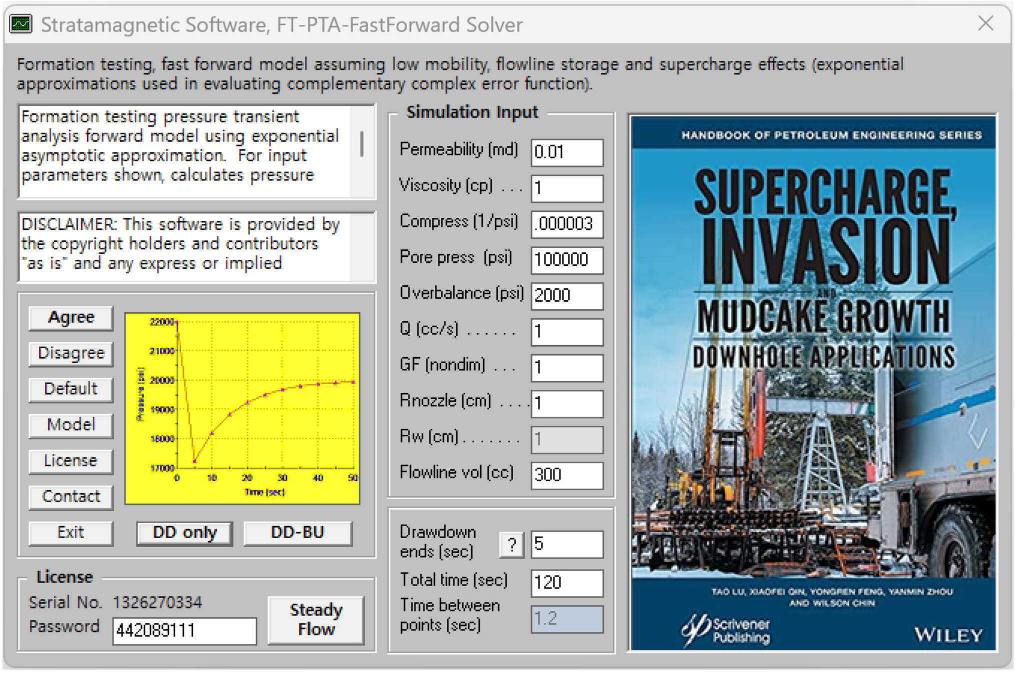

Figure 6 Mobility = 0.01 md/cp input assumptions for forward analysis.

```
Fluid, formation, tool and pumping parameters ...

Formation permeability .......... (md):   0.1000E-01
Viscosity ...................... (cp):   0.1000E+01
Liquid compressibility ....... (1/psi):   0.3000E-05
Pore pressure ................. (psi):   0.1000E+06
Overbalance pressure .......... (psi):   0.2000E+04
Volume flow rate ............. (cc/s):   0.1000E+01
Probe radius .................. (cm):   0.1000E+01
Geometric factor ..... (dimensionless):   0.1000E+01
Effective radius ............... (cm):   0.1000E+01
Flowline volume ................ (cc):   0.3000E+03
Total simulation time ......... (sec):   0.1200E+03
Graph every N sec, where "NSEC" equals:   0.1000E+01
```

T(sec)	P(psi)
0.0	102000.
1.0	100875.
2.0	99761.
3.0	98657.
4.0	97564.
5.0	96482.
6.0	95409.
7.0	94347.
8.0	93295.
9.0	92252.
10.0	91220.
20.0	81420.
30.0	72511.
40.0	64411.
50.0	57048.
60.0	50353.
70.0	44268.
80.0	38735.
90.0	33705.
100.0	29133.
110.0	24976.
120.0	21197.

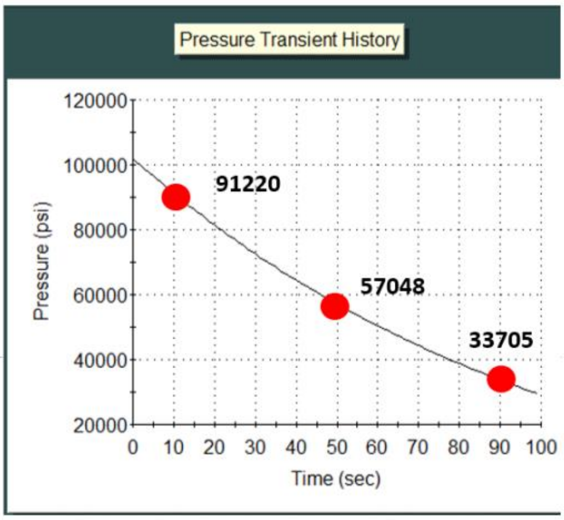

Figure 7 Computed forward pressure response at single pumping probe.

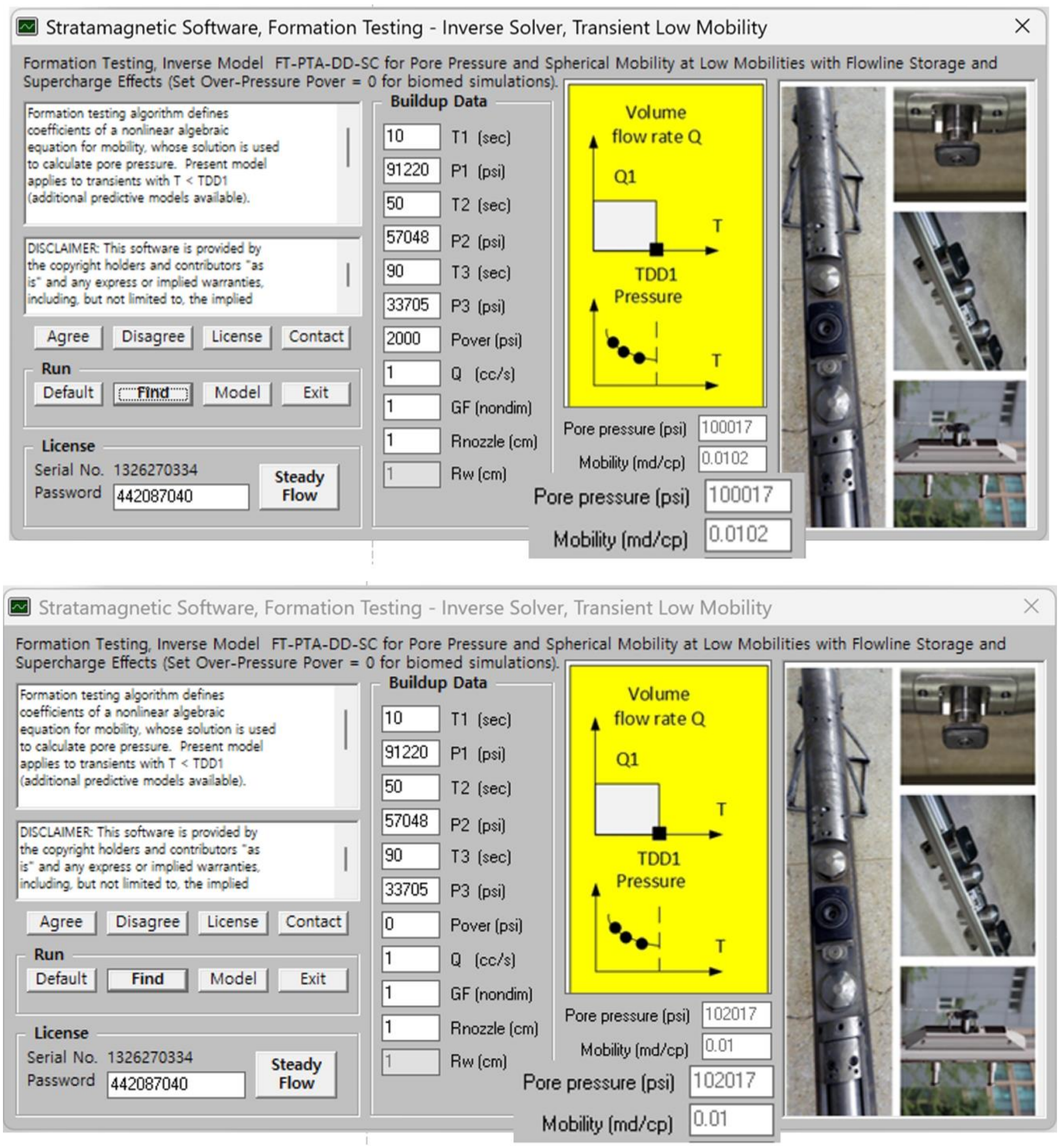

Figure 8 Mobility = 0.01 md/cp calculation. Note ϕ, c, C and V inputs are not required. *Upper*, P_{over} = 2,000 psi is inputted, predictions P_0 = 100,017 psi and mobility = 0.0102 md/cp both correct (inputs were 100,000 and 0.01). *Lower,* assumed P_{over} = 0 psi is incorrect, corresponding to conventional GeoTap™ type simulators. The prediction P_0 = 102,017 psi is incorrect by 2,017 psi, while the predicted mobility = 0.01 md/cp is correct. This correct value, however, is fortuitous as we will conclude from later examples.

3.3 Example 3: Mobility = 0.1 md/cp Calculations (Very Tight Zone)

In Example 3, we first solve our "FT-PTA-FastForward (forward) Simulator" assuming a mobility of 0.1 md/cp in Figure 9. In the computed results for this single source probe problem, we arbitrarily select three widely separated red "pressure and time" pairs. Figure 10 shows these inputs in "inverse" code FT-PTA-DD-SC along with other parameters that do *not* include ϕ, c, C and V. We entered the overbalance pressure P_{over} = 2,000 psi in the upper inverse menu of Figure 11. The caption indicates excellent results for mobility and pore pressure. In the lower inverse menu, we entered an incorrect P_{over} = 0 psi and obtained incorrect results.

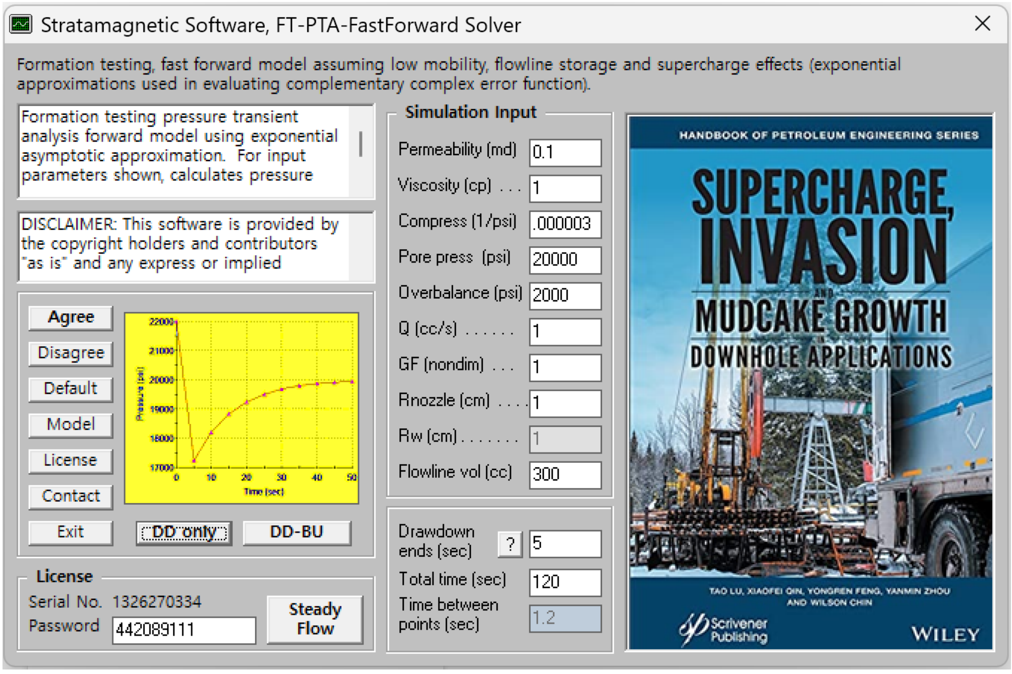

Figure 9 Mobility = 0.1 md/cp input assumptions for forward analysis.

```
FORMATION TESTER, FORWARD PRESSURE TRANSIENT MODEL
Forward pressure transient predictions for drawdown-only
applications, for low mobility, isotropic, supercharged
flows where flowline storage is not negligible.

Fluid, formation, tool and pumping parameters ...

Formation permeability ......... (md):   0.1000E+00
Viscosity ...................... (cp):   0.1000E+01
Liquid compressibility ....... (1/psi):  0.3000E-05
Pore pressure ................. (psi):   0.2000E+05
Overbalance pressure .......... (psi):   0.2000E+04
Volume flow rate ............. (cc/s):   0.1000E+01
Probe radius ................... (cm):   0.1000E+01
Geometric factor ..... (dimensionless):  0.1000E+01
Effective radius ............... (cm):   0.1000E+01
Flowline volume ................ (cc):   0.3000E+03
Total simulation time ......... (sec):   0.1200E+03
Graph every N sec, where "NSEC" equals:  0.1000E+01
```

T(sec)	P(psi)
0.0	22000.
1.0	20758.
2.0	19630.
3.0	18604.
4.0	17671.
5.0	16823.
6.0	16052.
7.0	15351.
8.0	14713.
9.0	14134.
10.0	13607.
20.0	10371.
30.0	9123.
40.0	8642.
50.0	8456.
60.0	8385.
70.0	8357.
80.0	8346.
90.0	8342.
100.0	8341.
110.0	8340.
120.0	8340.

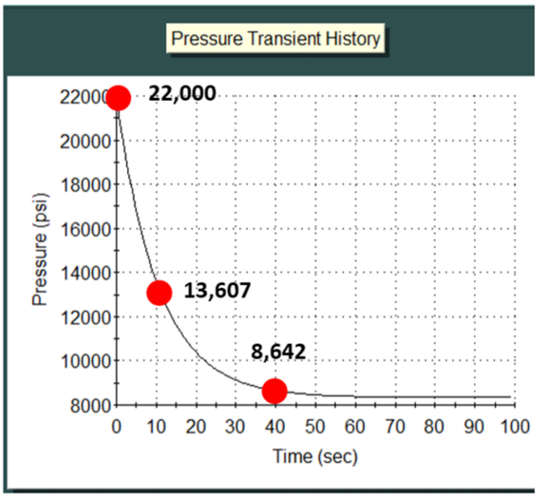

Figure 10 Computed forward pressure response at single pumping probe.

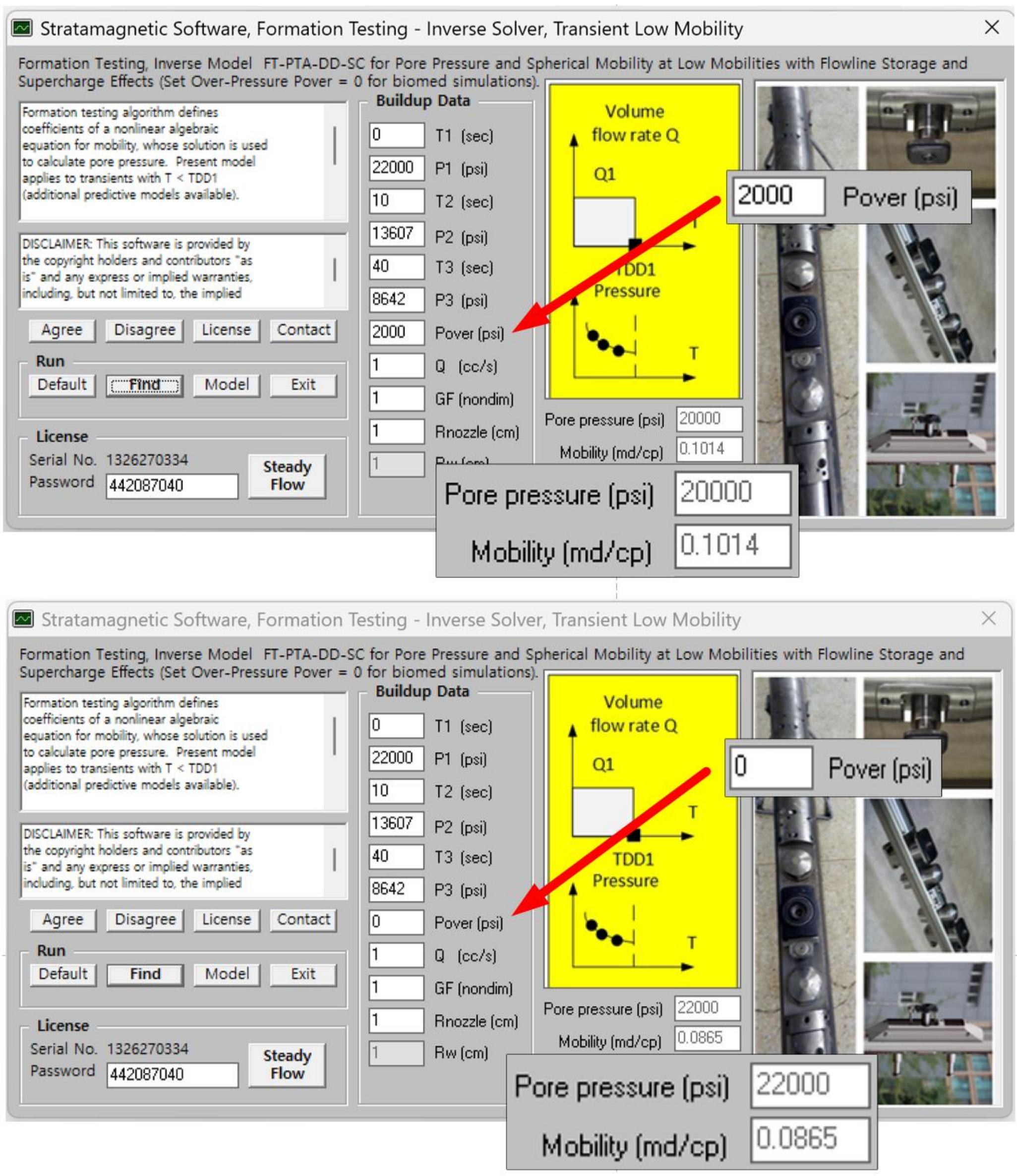

Figure 11 Mobility = 0.1 md/cp calculation. Note ϕ, c, C and V inputs not required. Upper, P_{over} = 2,000 psi inputted, predictions P_0 = 20,000 psi and mobility = 0.1014 md/cp both correct. Lower, P_{over} = 0 psi incorrect, predictions P_0 = 22,000 psi and mobility = 0.0865 md/cp both incorrect. Thus, forward and inverse algorithms are physically and mathematically consistent.

3.4 Example 4: Mobility = 1 md/cp Calculations (Tight Zone)

A work flow identical to that of the above examples is used, except that we take a mobility = 1 md/cp in the forward simulator of Figure 12. Synthetic pressure results appear in Figure 13. Inverse results are shown in Figure 14. As before, when the correct overbalance pressure P_{over} is entered in the inverse menu, excellent permeability and pore pressure results are obtained. However, when taken incorrectly as “0,” the predicted permeability and pore pressure are both inaccurate. In this and prior examples, our assumed over-pressures of 2,000 psi are realistic, following measured levels reported Rourke et al. [9].

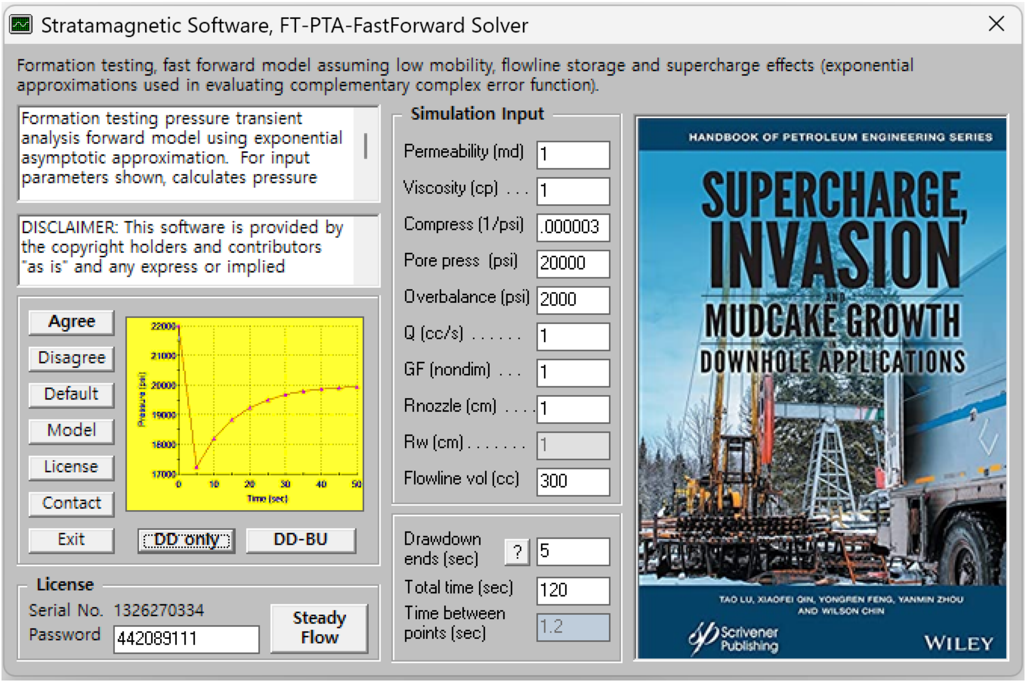

Figure 12 Mobility = 1.0 md/cp input assumptions for forward analysis.

```
FORMATION TESTER, FORWARD PRESSURE TRANSIENT MODEL
Forward pressure transient predictions for drawdown-only
applications, for low mobility, isotropic, supercharged
flows where flowline storage is not negligible.

Fluid, formation, tool and pumping parameters ...

Formation permeability ......... (md):   0.1000E+01
Viscosity ...................... (cp):   0.1000E+01
Liquid compressibility ....... (1/psi):   0.3000E-05
Pore pressure ................. (psi):   0.2000E+05
Overbalance pressure .......... (psi):   0.2000E+04
Volume flow rate ............. (cc/s):   0.1000E+01
Probe radius ................... (cm):   0.1000E+01
Geometric factor ..... (dimensionless):   0.1000E+01
Effective radius ............... (cm):   0.1000E+01
Flowline volume ................ (cc):   0.3000E+03
Total simulation time ......... (sec):   0.1200E+03
Graph every N sec, where "NSEC" equals:   0.1000E+01
```

T (sec)	P (psi)
0.0	22000.
1.0	20055.
2.0	19305.
3.0	19016.
4.0	18904.
5.0	18861.
6.0	18844.
7.0	18838.
8.0	18836.
9.0	18835.
10.0	18834.
11.0	18834.
12.0	18834.
13.0	18834.
14.0	18834.
15.0	18834.
16.0	18834.
17.0	18834.
18.0	18834.
19.0	18834.
20.0	18834.

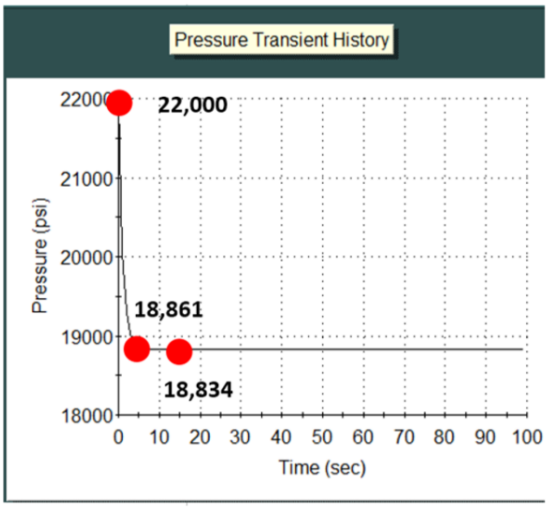

Figure 13 Computed forward pressure response at single pumping probe.

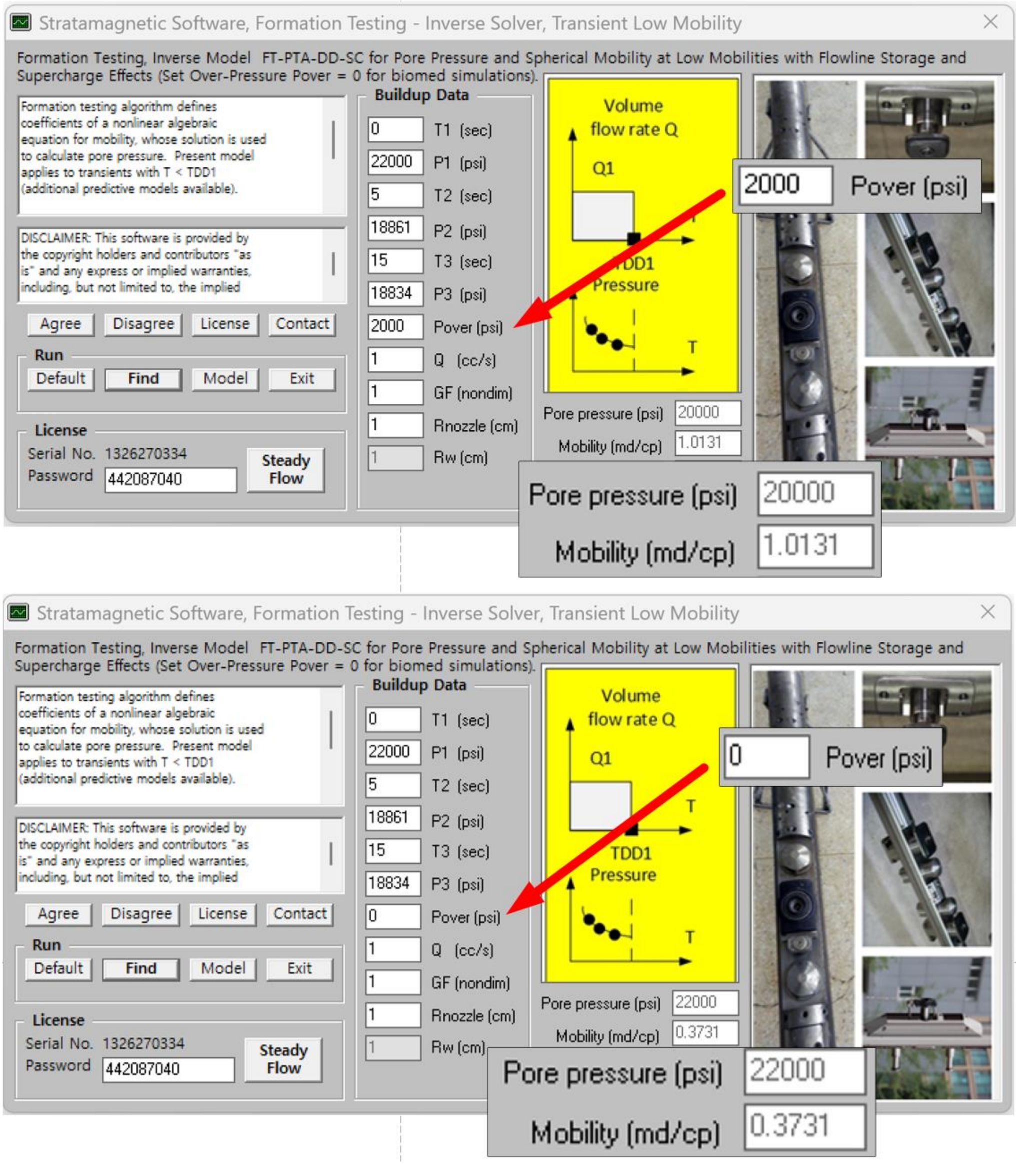

Figure 14 Mobility = 1.0 md/cp calculation. Note ϕ, c, C and V inputs not required. *Upper*, P_{over} = 2,000 psi inputted, predictions P_0 = 20,000 psi and mobility = 1.0131 md/cp both correct. *Lower*, P_{over} = 0 psi is incorrect (as in conventional inverse models), predictions P_0 = 22,000 psi and mobility = 0.3731 md/cp are both incorrect.

3.5 Example 5: Mobility = 10 md/cp Calculations (High Mobility)

This final Example 5 is very instructive. A work flow identical to that of the above examples is used, except that we take a high value of mobility = 10 md/cp in the forward simulation of Figure 15. Such high values imply very rapid equilibrations to steady state. At first, the flowline volume of 300 cc used in prior examples was taken, leading to measurement time windows much smaller than 1 sec. This means that identifying three useful (pressure, time) pairs for inverse problem input would be impossible. How can this situation be corrected? We turn to Equations 1-4, and in particular the last, with $(4\pi R_w^2 k/\mu)\partial P(R_w,t)/\partial r - VC\partial P/\partial t = Q_0$. *It can be shown mathematically that time window width increases as the product VC increases, while predicted pore pressures and permeabilities remain unchanged.* It is possible to prove this from the closed form expressions in

Equations 9 and 10. Petroleum engineers have long recognized that large flowline volumes are undesirable because "they distort true pressure profiles" (formation tester designers minimize the value of V where possible). While pressure profile shapes do change, their understanding that predicted properties are likewise affected is incorrect. This realization is useful in many industrial applications and we have taken advantage of it in related mechanical design problems. For now, Figure 15 shows our selection of a highly exaggerated 30,000 cc. The original time window, much less that 1 sec, is increased to about 10 sec as seen from Figure 16. The caption in Figure 17 concludes that inputting the known overbalance of 2,000 psi leads to the correct 100 psi pore pressure and an acceptable mobility of 10.4 (versus 10 md/cp). However, entering P_{over} = 0, leads to 2,100 psi and 0.559 md/cp, which are both incorrect. This example, using some exaggerated parameters, has demonstrated some useful physical properties underlying Equations 1-4.

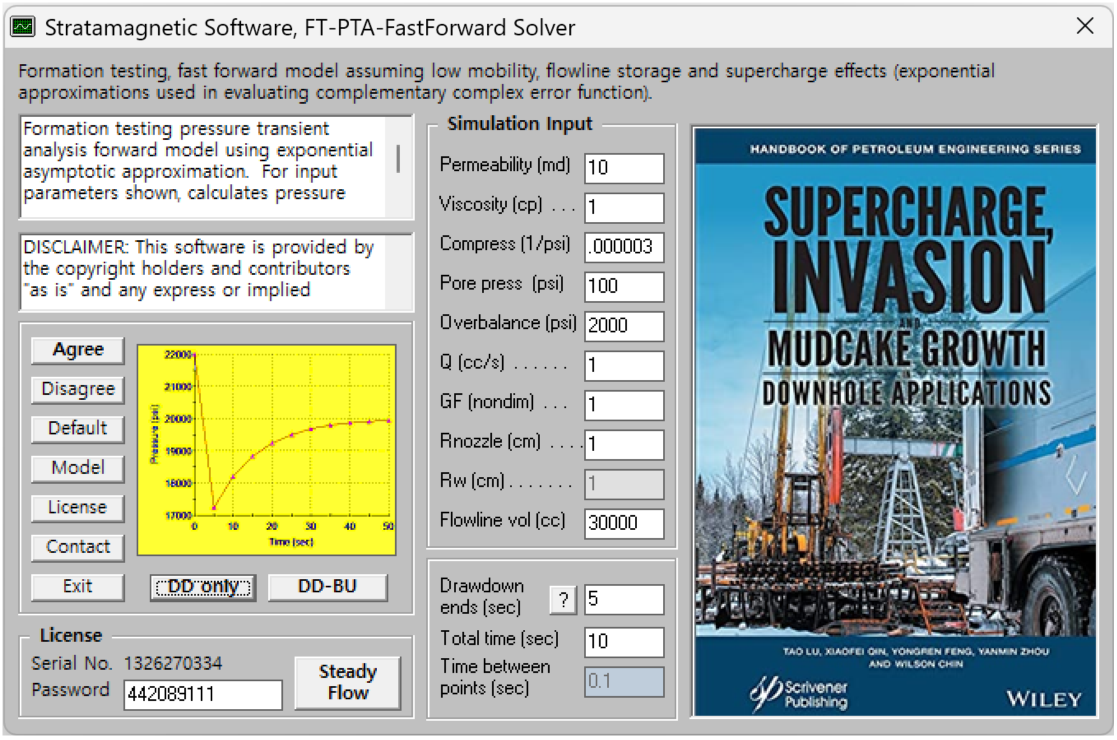

Figure 15 Mobility = 10 md/cp input assumptions for forward analysis.

T (sec)	P (psi)
0.0	2100.
1.0	1908.
2.0	1733.
3.0	1574.
4.0	1429.
5.0	1298.
6.0	1178.
7.0	1070.
8.0	971.
9.0	881.
10.0	800.

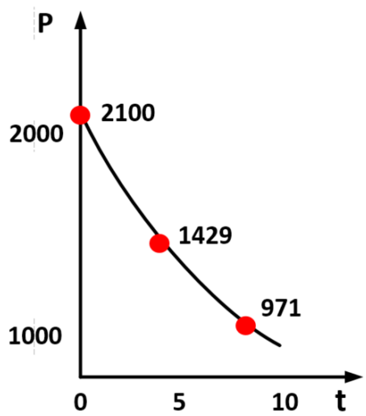

Figure 16 Computed forward pressure response at single pumping probe.

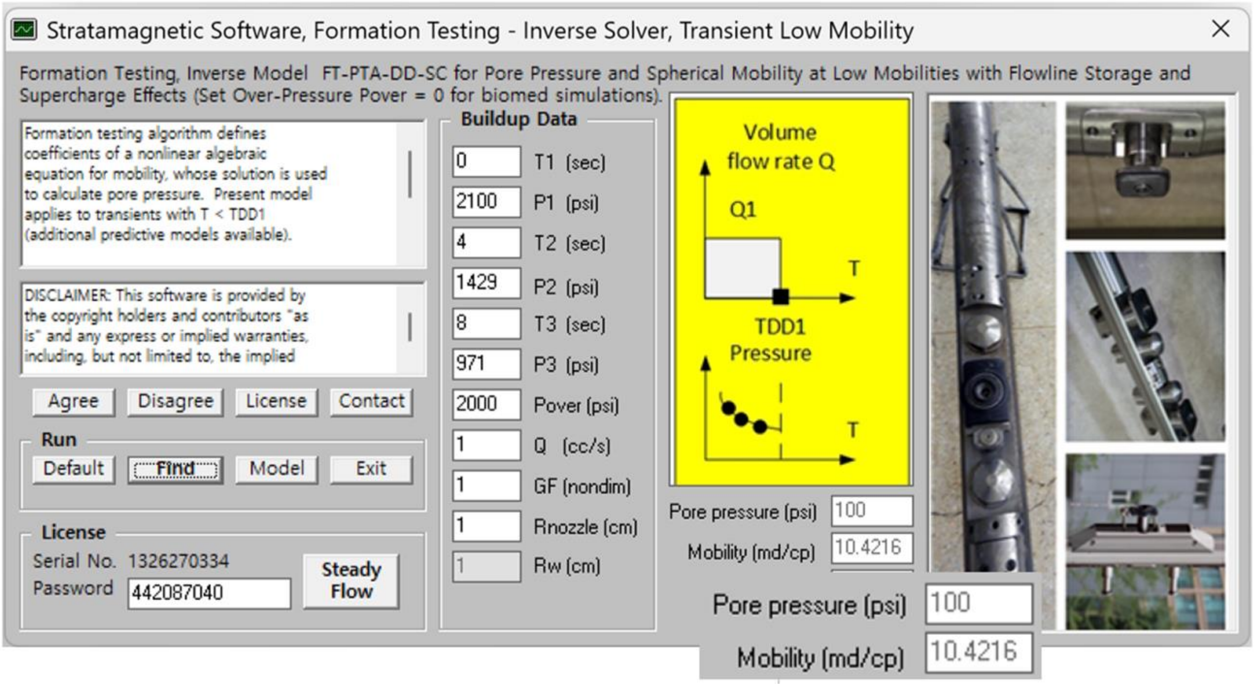

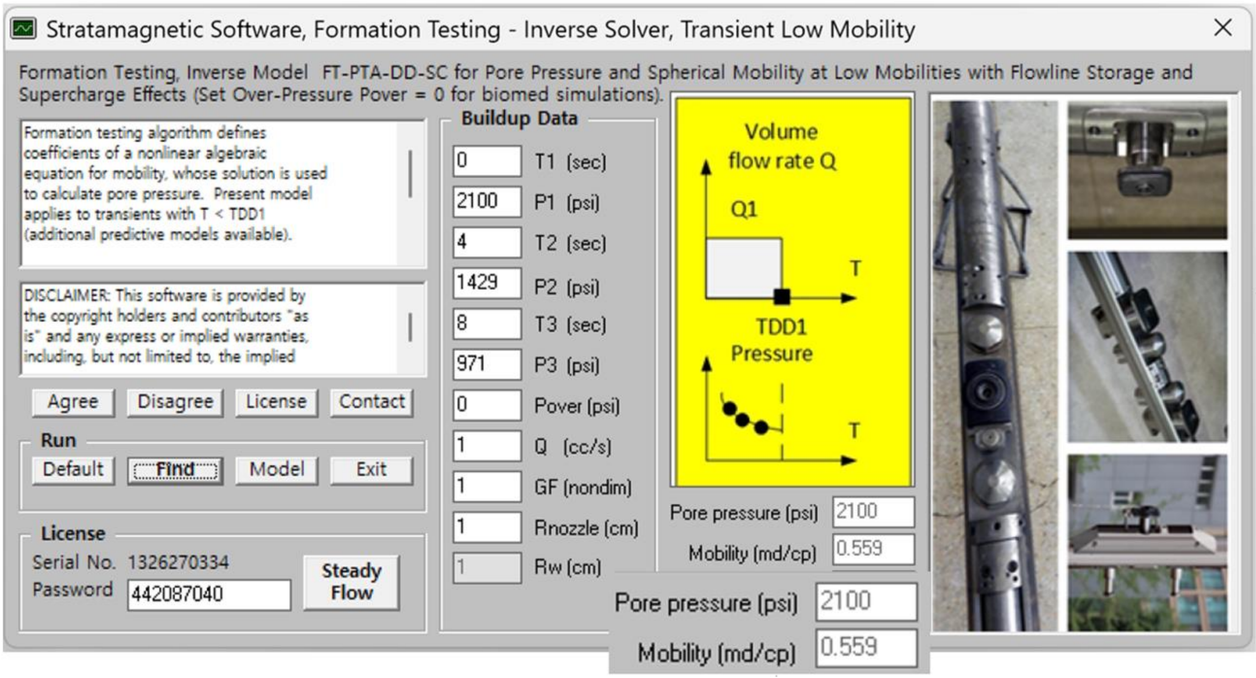

Figure 17 Mobility = 10 md/cp calculation. *Upper*, inputting the known overbalance of 2,000 psi leads to the correct 100 psi and an acceptable mobility of 10.4 (versus 10 md/cp). *Lower*, entering P_{over} = 0, however, leads to 2,100 psi and 0.559 md/cp, both incorrect.

4. Discussion

We developed an *exact* “forward”” simulator that calculates pressures given mobility, pore pressure and excess pressure values, designed to assist job planning under overbalanced conditions. Next, using three selected (pressure, time) pairs calculated at the source probe location, we validated our *approximate* "inverse" solver, based on independent asymptotic expansions, which predicts mobility and pore pressure inputs accurately. This overbalance *single-probe* test method reduces to zero-supercharge models conventionally used, e.g., Halliburton's GeoTap™ and COSL's EFDT™, also designed by this author, as well as reducing to BakerHughes' FRA™ (Formation Rate Analysis) in Kasap [26] and Kasap et al. [27]. Our validation examples showed that knowledge of overbalance pressure, e.g., numerous available from expired patents and industry literature, is required for accurate predictions. Note that our method also applies to underbalanced drilling, although that subject is not covered here.

Again, the predictions for the "effective permeability" $k_{eff} = kh^{2/3}kv^{1/3}$ apply to single-probe tools and do not require dual probe capabilities for use. Both individual kh and kv values, useful in hydraulic fracturing, wellbore stability, infill drilling and reservoir engineering, can be obtained from dual axial probe measurements using a real-time method to be presented in a future *Journal of Energy and Power Technology*. While the "$P(r,t = 0) = P_0 + Z/r$" elllipsoidal flow approach presented here may appear to be crude, it does offer rapid and stable estimates suitable in field work where input parameters for other aspects of the problem shown in Figure 1 and Figure 2 are generally not available. We emphasize that detailed simulation models including borehole size, dynamic mudcake growth, overbalance and wellbore invasion, circular, oval and slotted nozzle geometries, multiple direct and focusing probes, different pumping rates and schedules, and other effects, *are* available for single phase and as well as pressure-coupled miscible multiphase flows. These more sophisticated solvers are described in Chin [15] and require input parameters not generally available, e.g., mud cake growth factors under dynamic invasion. They are designed for detailed analysis while the approximate method in this paper addresses the needs of field practitioners who need answers when little wellbore information is available. Figures 18-21 show menus for single-probe and also azimuthally separated multiprobe tools addressed in Chin [15], typical spatial pressure and contamination plots, main probe versus focusing probe dynamics, and so on, and are offered here for completeness without further explanation. They show that more accurate simulation tools have been developed, although they may not be convenient in field work, again where detailed inputs are not yet available. The more complete models play useful roles for immediate interpretation and drilling planning once operational demands and rig site constraints are no longer a factor.

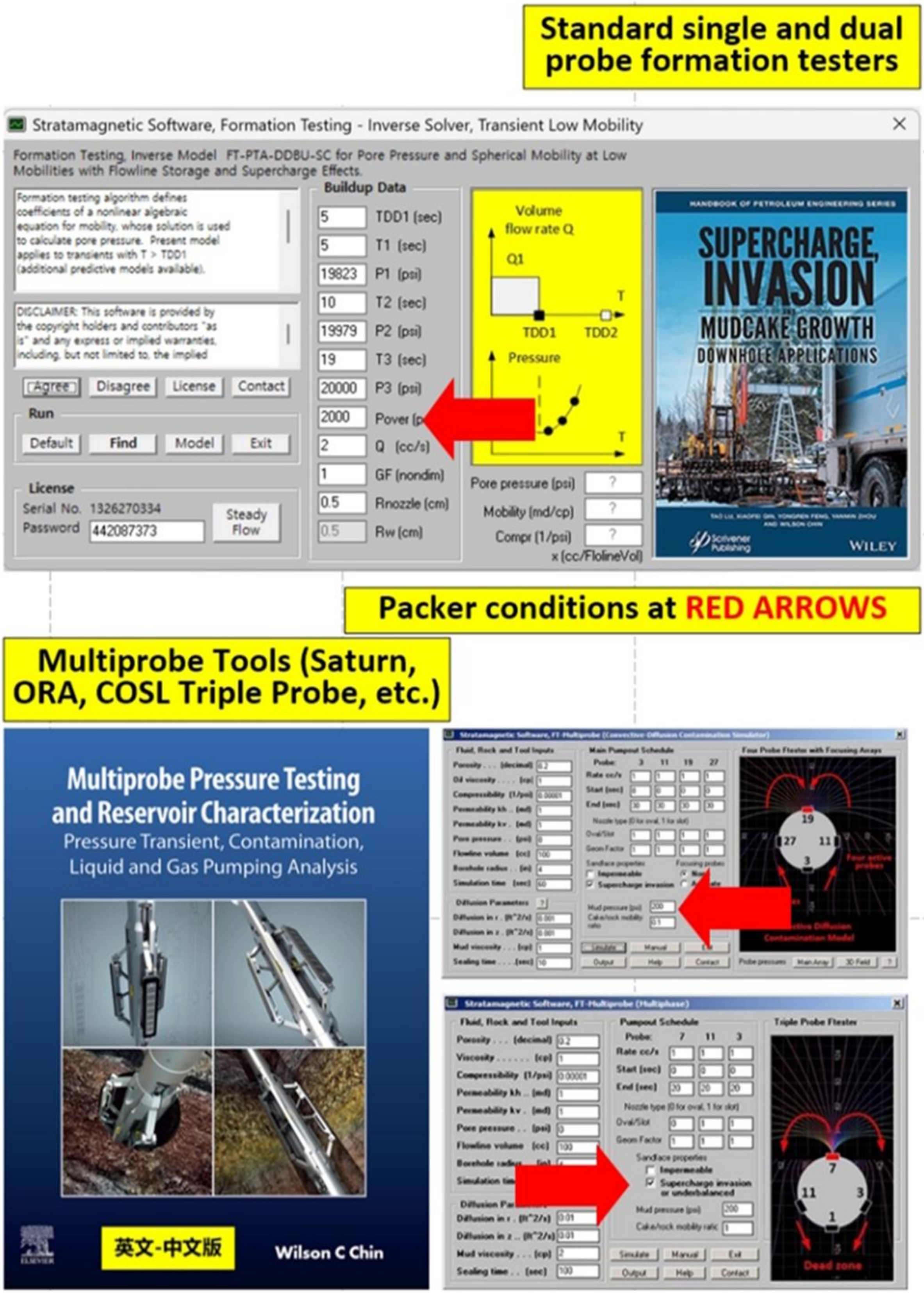

Figure 18 Upper screen-Single-probe model (this paper). Lower screen-multiprobe model from Chin [15], azimuthal probe menu with arrows showing supercharge input boxes.

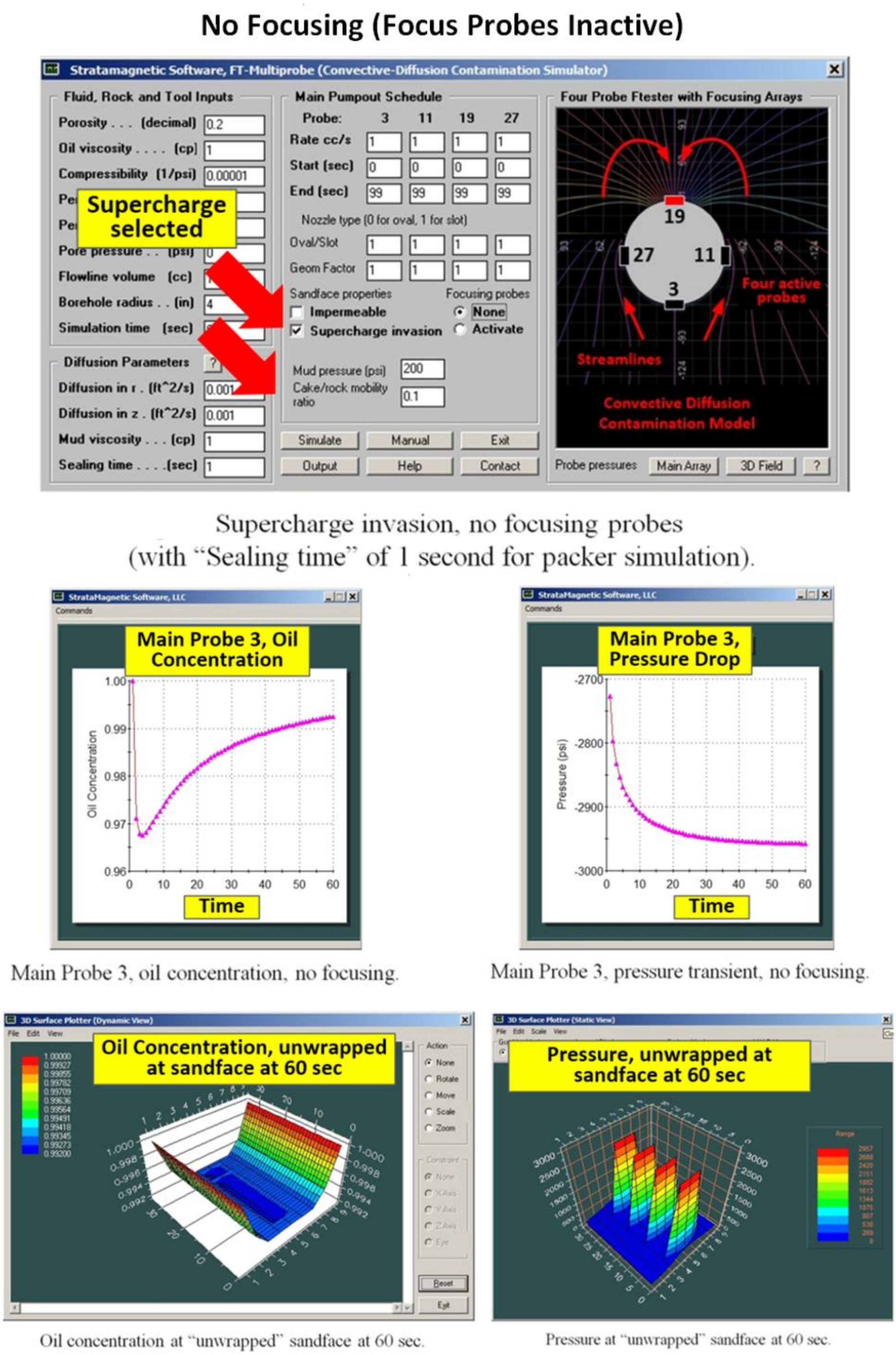

Figure 19 Azimuthal multiprobe concentrations and pressures without focusing, note oil concentration decreases at first, then increases with time as growing mudcake seals formation.

Two Focusing Rows (Focus Probe *and* Supercharge Options Activated)

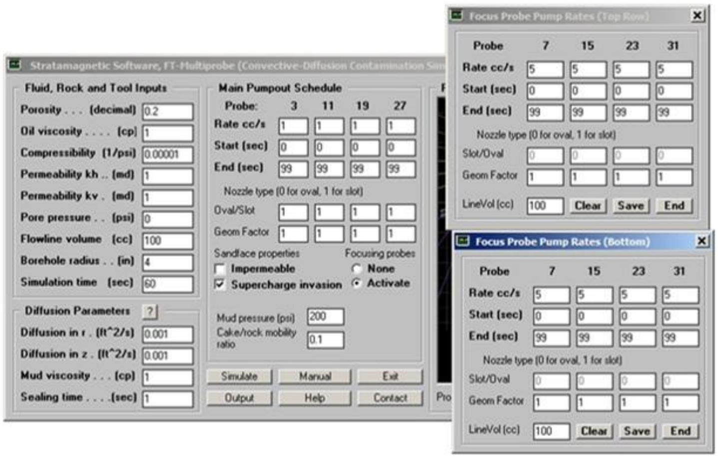

Simulation with activated focusing probes.

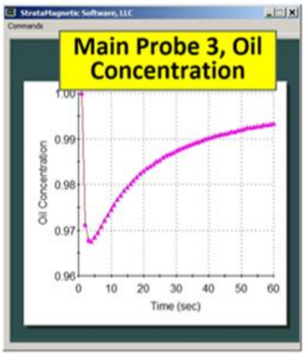

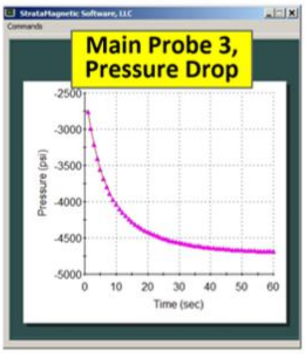

Main Probe 3, oil concentration, with focusing. Main Probe 3, pressure transients, with focusing.

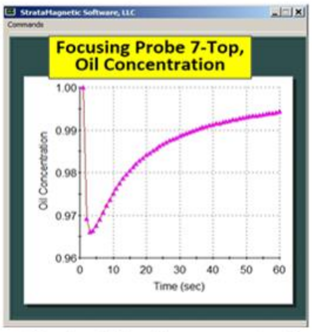

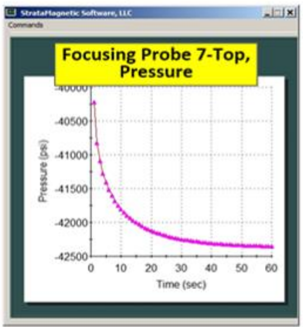

Focusing Probe 7T, oil concentration. Focusing Probe 7T, pressure transients.

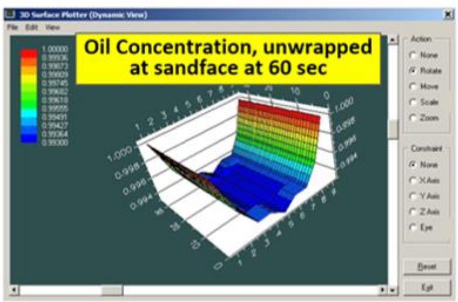

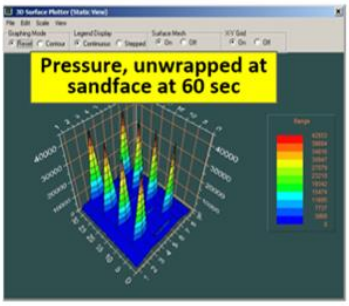

Oil concentration at t = 60 sec (rotatable plot). Pressure field at t = 60 sec.

Figure 20 Azimuthal multiprobe concentrations and pressures with focusing. Simulations show that two focusing probe rows in this case did not function effectively per manufacturer’s claims.

System	Probes	$\Delta\theta$ Grids	Description*
1 mprobe (dual)	1 active & 1 passive at 180°	12	Single-phase liquid, one pump nozzle, one 180° observer, impermeable sandface, underbalance or invasion, mimics MDT™
2 mprobe (quad)	4 active	24	Single-phase liquid, four pump nozzles, impermeable sandface, UB or invasion, mimics Saturn™ operation
3 mprobe (focus)	4 active & 2 focus row	32	Single-phase liquid, main array with two more rows (12 independent probes in all), useful for research analyses
4 mprobe (contam)	4 active & 2 rows for focusing	32	Multiphase (miscible) contamination mimics ORA™ operation for coupled pressure and oil concentration
5 mprobe (triplet)	3 active 1 passive	12	Single-phase liquid, three *identical* nozzles, different rates and start-stop times, impermeable sandface, UB or invading, mimics original COSL triple-probe tool
6 mprobe	3 active 1 passive	12	Single-phase liquid, three *different* nozzles, different rates and start-start times, and geometric factors, impermeable sandface, UB or invading, mimics COSL triple-probe
7 mprobe (3-contam)	3 active 1 passive	12	Multiphase liquid, pressure and contamination modeling, three different nozzles, different rates and start-start times, geometric factors, impermeable sandface, UB or invading, mimics COSL triple-probe
8 mprobe (3-gas)	3 active 1 passive	12	Single-phase nonlinear gas pumping, general thermodynamics, similar to System 6's COSL "mprobe" for liquids
9 mprobe (4-gas)	4 active	24	Single-phase nonlinear gas pumping, gen'l thermodynamics, similar to System 2 Saturn "mprobe(quad)" for liquids

Figure 21 Multiprobe software simulator system models.

This paper again deals with single-phase, single-probe models, applicable when two-phase effects are minimal. For multiprobe, multiphase flow discussions developed in Chin [15], refer to *Handbook of Fluid Mechanics*, Streeter [4] for elementary ideas, while for additional formation testing methods, see *Fundamentals of Formation Testing* [33]. Multiprobe simulations in Figure 18(lower) are discussed in this author's *Multiprobe Pressure Testing and Reservoir Characterization* [15]. For completeness, Figure 19 and Figure 20 reproduce a packer application relevant to the problem addressed in this paper. Figure 19 shows results when focusing probe arrays are inactive, while Figure 20 shows results when both focusing probe rows are activated.

Figure 21 summarizes nine System Models applicable to Schlumberger Saturn™ (4 slot probes), ORA™ (4 main slot probes, two surrounding rows of circular probes, for a total of 12 probes), and COSL's EFDT™ (3 probe) tool, and patented designs from other manufacturers. System 1 specifically addresses MDT™ applications, with active and passive probes positioned diametrically opposite each other in the well. Computed pressure fields for such runs do not always agree with "ideal source probe" infinite media runs because the presence of boreholes with non-zero radii implies a completely different problem. All the methods in Chin [15] model supercharge. Figure 19 and Figure 20 show results for coupled pressure and miscible contamination analysis. Additional information can be obtained by author email at stratamagnetic.software@outlook.com or by downloading related references from www.stratamagnetic.com.

5. Conclusions

The single-probe, infinite media, transversely isotropic, elliptical source models for forward and inverse supercharged flows formulated and validated in this paper, together with the azimuthal multiphase models for coupled pressure and contamination referenced in Section 4 (e.g., see Chin [15]) provide a complete suite of pressure analysis tools for packer applications and problems with dynamic invasion, transient mudcake grown, viscosity averaging in miscible multiphase flows, and high overbalance pressures. Recently, we also developed a method to predict both kh and kv individually for dual probe tools. This capability, useful in hydraulic fracturing, infill drilling, wellbore stability and reservoir engineering, is summarized in Chin [38] recently appearing in the *Journal of Energy and Power Technology*. The library of analysis methods now permits petroleum engineers and well logging analysts to plan formation testing jobs, understand test consequences, as well as perform comparative studies relating benefits and limitations of different manufacturers' tools. The methods describe were developed with special focus on consistency with fluid physics, accuracy, numerical stability and computational speed, and should offer a robust platform for rig site engineering calculations.

Author Contributions

Wilson Chin formulated, solved and validated both forward and inverse supercharge models without assistance from other individuals or AI tools. Wilson earned his Ph.D. from MIT and M.Sc. from Caltech, in Applied Math, Fluid Mechanics and Physics. From 2014 to 2024, he authored six formation testing books with John Wiley & Sons and Elsevier Science. In 1997, he developed Halliburton's real-time permeability prediction method, GeoTap™. At China Oilfield Services Ltd a decade later, he developed the "rational polynomial" permeability algorithms used in COSL's EFDT™ Enhanced Formation Dynamics Tester. This suite, a predecessor to the supercharge method given here, recently won a "Spotlight on New Technology Award" at the OTC Asia 2026 Conference in Kuala Lumpur, Malaysia.

Funding

This research was funded internally by Stratamagnetic Software, LLC.

Competing Interests

The author declares that no competing interests exist.

AI-Assisted Technologies Statement

Artificial intelligence (AI) tools were not used in deriving or illustrating any of the new analysis methods, nor were they used in grammatical correction, linguistic clarity or related purposes. All scientific content, data interpretation, and conclusions in the paper were developed independently of AI tools and represent original research performed solely by the author.

References

1. Muskat M. Flow of homogeneous fluids. Ann Arbor, MI: J. W. Edwards; 1937.
2. Dake LP. Fundamentals of reservoir engineering. Amsterdam, Netherlands: Elsevier Science; 1978.
3. Scheidegger AE. The physics of flow through porous media. 3rd ed. Toronto, Canada: University of Toronto Press; 1974.
4. Streeter VL. Handbook of fluid dynamics. New York, NY: McGraw-Hill; 1961.
5. Yih CS. Fluid mechanics. New York, NY: McGraw-Hill; 1969.
6. Proett MA, Chin WC, Chen CC. Method of formation testing. Alexandria, VA: U.S. Patent; 1997.
7. Proett MA, Chin WC, Mandal B. Advanced permeability and anisotropy measurements while testing and sampling in real-time using a dual probe formation tester. Proceeding of the SPE Annual Technical Conference and Exhibition; 2000 October 01-04; Dallas, TX. Richardson, TX: SPE Paper.
8. Lee HJ. Simulation and interpretation of formation-tester measurements acquired in the presence of mud-filtrate invasion and geomechanical deformation. Austin, TX: The University of Texas at Austin; 2008.
9. Rourke M, Powell B, Platt C, Hall K, Gardner A. A new hostile environment wireline formation testing tool: A case study from the Gulf of Thailand. Prcoeedings of the SPWLA Annual Logging Symposium; 2006 June 04-07; Veracruz, Mexico. Houston, TX: SPWLA.
10. Chin WC. Formation testing: Supercharge, pressure testing, and contamination models. Hoboken, NJ: John Wiley & Sons; 2019.
11. Chin WC, Zhou Y, Feng Y, Yu Q, Zhao L. Formation testing: Pressure transient and contamination analysis. Hoboken, NJ: John Wiley & Sons; 2014.
12. Chin WC, Zhou Y, Feng Y, Yu Q. Formation testing: Low mobility pressure transient analysis. Hoboken, NJ: John Wiley & Sons; 2016.
13. Lu T, Qin X, Feng Y, Zhou Y, Chin WC. Supercharge, invasion and mudcake growth in downhole applications. Hoboken, NJ: John Wiley & Sons; 2021.
14. Lu T, Zhou M, Chin WC, Yang Y, Feng Y. Multiprobe pressure analysis and interpretation. Beverly, MA: Scrivener Publishing LLC.; 2021.
15. Chin WC. Multiprobe pressure testing and reservoir characterization: Pressure transient, contamination, liquid and gas pumping analysis. Amsterdam, Netherlands: Elsevier Science; 2024.
16. Abramowitz M, Stegun IA. Handbook of mathematical functions. Garden City, NY: Dover Publications; 1972.
17. Bateman H. Tables of integral transforms. New York, NY: McGraw-Hill; 1954.
18. Carnahan B, Luther H, Wilkes J. Applied numerical methods. Hoboken, NJ: John Wiley & Sons; 1969.

19. Churchill RV. Operational mathematics. New York, NY: McGraw-Hill; 1958.
20. International Mathematical and Statistical Libraries I. IMSL library reference manual, Vol 3, Chapter M. Minneapolis, MN: IMSL Inc; 1982.
21. Pipes LA. Applied mathematics for engineers and physicists. New York, NY: McGraw-Hill; 1958.
22. Press WH, Teukolsky SA, Vetterling WT, Flannery BP. Numerical recipes in fortran 77. 2nd ed. Cambridge, UK: Cambridge University Press; 1992.
23. Goode PA, Thambynayagam R. Permeability determination with a multiprobe formation tester. SPE Form Eval. 1992; 7: 297-303.
24. Horne RN. Modern well test analysis: A computer-aided approach. 2nd ed. Palo Alto, CA: Petro Way; 1995.
25. Joseph JA, Koederitz LF. Unsteady-state spherical flow with storage and skin. Soc Pet Eng J. 1985; 25: 804-822.
26. Kasap E. Fluid flow rate analysis method for wireline formation testing tools. Alexandria, VA: U.S. Patent; 1998.
27. Kasap E, Huang K, Shwe T, Georgi D. Formation-rate-analysis technique: Combined drawdown and buildup analysis for wireline formation test data. Soc Pet Eng J. 1999; 2: 271-280.
28. Moran J, Finklea E. Theoretical analysis of pressure phenomena associated with the wireline formation tester. J Pet Technol. 1962; 14: 899-908.
29. Peaceman DW. Fundamentals of numerical reservoir simulation. Amsterdam, Netherlands: Elsevier Science; 1977.
30. Proett MA, Waid MC. Wireline formation testing for low permeability formations utilizing pressure transients. Alexandria, VA: U.S. Patent; 1997.
31. Raghavan R. Well test analysis. Englewood Cliffs, NJ: PTR Prentice Hall, Englewood Cliffs; 1993.
32. Sabet MA. Well test analysis. Houston, TX: Gulf Publishing Company; 1991.
33. Schlumberger Staff. Fundamentals of formation testing. Sugar Land, TX: Schlumberger Marketing Communications; 2006.
34. SPWLA Staff. SPWLA wireline formation testing technology workshop. Proceeding of the 38th SPWLA Annual Symposium; 1997 June 15-18; Houston, TX. Houston, TX: Society of Professional Well Log Analysts.
35. SPWLA Staff. SPWLA formation testing: Applications and practices. Proceeding of the spring topical conference; 2004 March 28-April 1; Taos, NM. Houston, TX: Society of Professional Well Log Analysts.
36. Stanislav JF, Kabir CS. Pressure transient analysis. Englewood Cliffs, NJ: Prentice Hall, Englewood Cliffs; 1990.
37. Streltsova TD. Well testing in heterogeneous formations. Hoboken, NJ: John Wiley & Sons; 1988.
38. Chin WC. Real-time prediction of anisotropies kh and kv in dual axial probe formation testing. J Energy Power Technol. 2026; 8: 016.